

Quantum Transport of Massless Dirac Fermions in Graphene

Kentaro Nomura and A.H. MacDonald

Department of Physics, University of Texas at Austin, Austin TX 78712-1081, USA

(Dated: February 8, 2020)

Motivated by recent graphene transport experiments, we have undertaken a numerical study of the conductivity of disordered two-dimensional massless Dirac fermions. We find that in the short-range scattering case the minimum conductivity $\sigma_{\min} \approx (1/\pi) e^2/h$, while in the Coulomb scattering case $\sigma_{\min} \approx e^2/h$. We discuss the relationship between this finding and the experimental properties of graphene sheets, commenting on the possible roles of short-range, Coulombic, and topological-defect scatterers.

PACS numbers: 72.10.-d, 73.21.-b, 73.50.Fq

Introduction— Graphene can be described at low-energies by a four component massless Dirac-fermion model[1] (DFM) that has long attracted theoretical attention because of appealing properties including chiral anomalies[2, 3, 4, 5], randomness induced quantum criticality[6, 7, 8, 9], unusual electron-electron interaction effects[10, 11], and relevance to high T_c superconductors[10, 12]. Large momentum space Berry curvature near the Dirac point leads to zero-field quantum Hall effects[5], and to delocalized states in two-dimension that survive disorder[7]. The recent experimental realization of single-layer graphene sheets[13] has made it possible to confirm a number of theoretical predictions, including unusual half-integer quantum Hall effects[14, 15]. Indeed, there is good general agreement between theory[16] and experiment[14, 15] on the high-field transport properties of graphene. Zero-field experiments, on the other hand, have produced some surprises[14]. The main findings can be summarized as follows: i) graphene’s conductivity σ never falls below a minimum value (σ_{\min}) corresponding (approximately) to a conductance quantum (e^2/h) per channel, in contrast to theoretical[6, 7, 12, 17, 18, 19, 20] predictions that for the DFM $\sigma_{\min} \approx (1/\pi)e^2/h$; ii) in gate-doped graphene σ increases linearly with carrier density away from the Dirac point, implying a constant mobility $\mu = -\sigma/ne$ [14, 15] and not the constant conductivity predicted for the Boltzmann transport regime[19]; and iii) expected[21, 22] weak-(anti)localization effects are strongly suppressed[23]. Although these surprises have inspired a number of theoretical studies[20, 24], the source of the discrepancies between experiment and DFM theoretical predictions has not yet been conclusively identified.

In this Letter we point out that these three features of graphene transport data can *all* be explained by assuming that the disorder potential in graphene is dominated by long-range rather than short-range scatterers. (A δ -correlated disorder model has been adopted in most previous theoretical work[6, 7, 12, 17, 18, 19, 20] as a practical simplification.) In a previous paper[25], we used Boltzmann transport theory to point out that the

linear dependence of conductivity on carrier density in graphene can be explained by Coulomb scatterers. Since Boltzmann theory is only reliable in doped graphene, a fully quantum mechanical approach is required to address the minimum conductivity σ_{\min} which occurs at the Dirac point. In this Letter we use numerical finite-size Kubo formula calculations to estimate the conductivity and find that for Coulombic scatterers the DFM $\sigma_{\min} \approx e^2/h$ (in agreement with graphene experiment if inter-channel scattering is unimportant) while short-range scatterers lead to $\sigma_{\min} = (1/\pi)e^2/h$ as predicted by theory[6, 7, 12, 17, 18, 19, 20]. For finite doping, our numerical conductivities exhibit a size dependence that is consistent with predicted weak-antilocalization behavior[21] for both Coulomb and short-range scatterers, but is suppressed when a random vector potential is introduced to model topological defects[26, 27, 28, 29, 30].

Massless Dirac Model— Graphene’s honeycomb lattice has two atoms per unit cell on sites labeled A and B. The low-energy band structure consists of Dirac cones located at the two inequivalent Brillouin zone corners K and K' :

$$H_K = \hbar v \boldsymbol{\sigma} \cdot \mathbf{k} = v \hbar \begin{pmatrix} 0 & k_x - ik_y \\ k_x + ik_y & 0 \end{pmatrix}, \quad (1)$$

and $H_{K'} = \hbar v \boldsymbol{\sigma}^t \cdot \mathbf{k}$, where v is the graphene Fermi velocity and the Pauli matrices $\boldsymbol{\sigma}$ act on the sublattice degrees of freedom A and B. For each wavevector \mathbf{k} , Eq.(1) has two eigenstates $|\mathbf{k}, \pm\rangle = (|\mathbf{k}, A\rangle \pm e^{i\phi} |\mathbf{k}, B\rangle)/\sqrt{2}$, where $\phi \equiv \tan^{-1}(k_y/k_x)$, and eigenenergies $E_{\mathbf{k}, \pm} = \pm v|\mathbf{k}|$.

Boltzmann theory for doped graphene— We start by briefly reviewing Boltzmann transport theory applied to graphene since this consideration motivates the introduction of long-range disorder models. The Boltzmann conductivity $\sigma_0 = (e^2/h) (2E_F \tau/\hbar) = (e^2/h) 2k_F l$ is proportional to the transport relaxation time τ_0 . For short-range scatterers the Born approximation gives $\hbar/\tau_0 = 2\pi \overline{V^2} \rho_F = (n_i u^2/\hbar v^2) |E_F|$ [19, 21], where $V(\mathbf{r}) = u \sum_i^{N_i} \delta(\mathbf{r} - \mathbf{R}_i)$ is the disorder potential, $\overline{V^2} = N_i u^2$, $N_i = n_i L^2$ is the number of scatterers, L is the size of the system, and ρ_F the density of states at the Fermi

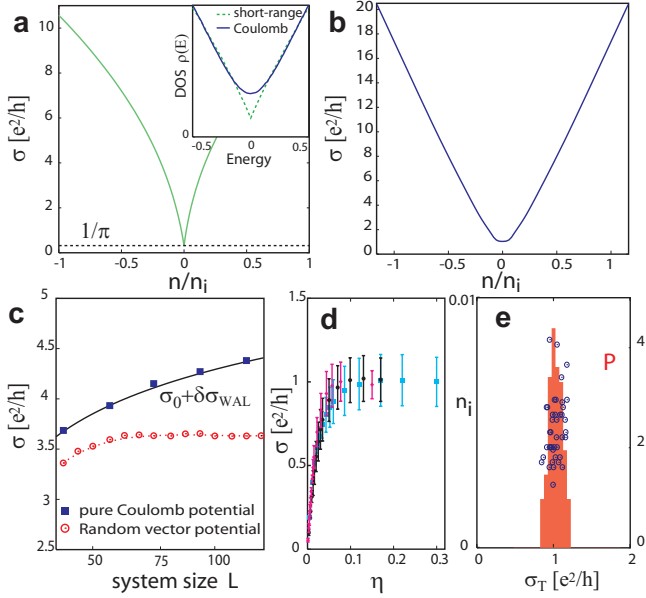


FIG. 1: DFM conductivities for (a) short-range scatterers and (b) screened Coulomb scatterers. The inset of (a) compares the densities of states for short-range and Coulomb cases. (c) Size dependence of the conductivity for doped graphene in the absence (blue boxes) and presence (red circles) of the random vector potential described in the text. In both cases $k_F l \simeq 7$. (d) Kubo formula conductivities at the Dirac point for three different system sizes as a function of η for Coulomb scatterers. (e) Thouless conductivities at the Dirac point as a function of the density of Coulomb scatterers.

level. When the range of the impurity potential is much longer than the lattice spacing of graphene, intervalley scattering is unimportant[19, 21]. Note that σ_0^s is independent of the carrier density n . Experiment, on the other hand, finds that the mobility $\mu = -\sigma/ne$ in graphene is nearly constant except at very low-densities. One plausible explanation for this behavior is that Dirac fermion scattering is dominated by Coulomb scattering from charged defects near the graphene plane, $V(\mathbf{r}) = \sum_i e^2/|\mathbf{r} - \mathbf{R}_i|$. Using Fermi's golden rule, and approximating the screened Coulomb interaction by[25] $U_{sc}(q) = (2\pi e^2)/(q + 4gk_F) \simeq (\hbar v\pi)/(2k_F)$ the Boltzmann conductivity for Coulomb interactions is $\sigma_0^c \simeq (4e^2/h) (n/n_i) 32/\pi$, proportional to density in agreement with experiment. Here $g = e^2/\hbar v$ is the effective *fine structure constant* used to characterize the ratio of Coulomb interaction and band energy scales in graphene. ($g \simeq 3$ in vacuum and $\simeq 1$ when the graphene sheet is placed on a dielectric substrate.) Note that the Boltzmann conductivity for Coulomb scatterers vanishes as $n \rightarrow 0$.

Linear response theory for the Dirac fermion – Our numerical results for zero-field transport are summarized in Fig.1. The results were obtained by evaluating the

finite-size Kubo formula:

$$\sigma = -\frac{i\hbar e^2}{L^2} \sum_{\alpha, \alpha'} \frac{f(E_\alpha) - f(E_{\alpha'})}{E_\alpha - E_{\alpha'}} \frac{\langle \alpha | v_x | \alpha' \rangle \langle \alpha' | v_x | \alpha \rangle}{E_\alpha - E_{\alpha'} + i\eta}, \quad (2)$$

where $\mathbf{v} = v\boldsymbol{\sigma}$ is the Dirac fermion velocity operator, $f(E)$ is the Fermi-Dirac function at $T = 0$, and $|\alpha\rangle$ denotes an eigenstate of the Dirac equation,

$$[-i\hbar v\boldsymbol{\sigma} \cdot \nabla + V(\mathbf{r})] \psi = E\psi \quad (3)$$

which we solve using a large momentum-space cutoff Λ . We estimate the bulk conductivity by evaluating Eq.(2) at a large number of η -values. The Kubo conductivity σ vanishes at both small and large η but there is a region where σ becomes finite and its dependence on η is relatively weak. We use the maximum of σ as a function of η to estimate the conductivity at a given system size L . For metals, including doped graphene, physical arguments suggest that $\eta \sim \hbar/T$ where T is the escape time from the small system studied numerically. It follows[31, 32] that $\eta \sim \langle \Delta E \rangle \sim \delta E \sigma/(e^2/h)$, where the Thouless energy $\langle \Delta E \rangle$ is the geometric mean of the eigenvalue difference between periodic and antiperiodic boundary conditions and $\delta E = 1/L^2 \rho_F$ is the level spacing at the Fermi level. The Thouless conductivity estimate, $\sigma_T = (e^2/h) (\pi/2) \langle \Delta E \rangle / \delta E$.

The reliability of the finite-size Kubo formula method described above is solidly established for diffusive metallic systems[32], while subtle issues remain in the case of insulators. The Dirac point is intermediate and we acknowledge this as an issue in the interpretation of our calculations. (The property that the Dirac point density of states is finite in the presence of disorder, as illustrated in the inset of Fig.1(a), should help validate the Kubo approach.) For this reason we have also evaluated the Thouless conductivity as a consistency check. A large number of numerical studies have demonstrated that the Thouless conductivity estimate, although perhaps not as accurate in the diffusive metal limit ($\sigma >> e^2/h$), is more universally applicable. It may be used for both delocalized and strongly localized states near band edges[33], and should therefore be reliable at the Dirac point. Figs.1 (d) and (e) establish the consistency of these two conductivity estimates and support the reliability of our numerical results for σ_{\min} . We find that the η -dependence of the Kubo formula estimate at the Dirac point is similar to that in a metal[32], indicating delocalized states. The dependence of disorder averaged σ on η is shown in Fig.1(c) for three different system sizes at the Dirac point.

Figure 1 compares Kubo conductivity estimate (a) the short-range scatterer and (b) the screened Coulomb scatterer cases. For the short-range disorder potential case, the density dependence of the conductivity is non-linear, approaching the constant Boltzmann conductivity for $|E_F| \gg \hbar/\tau$. The estimated value of

$\sigma_{\min} \simeq (1/\pi)e^2/h$ as predicted in earlier theoretical studies[6, 7, 12, 17, 18, 19, 20]. For the screened Coulomb scatterer case, on the other hand, the conductivity σ increases linearly with increasing density $|n|$ as Boltzmann theory predicts. At the Dirac point, however, the conductivity remains finite with the minimum value $\simeq e^2/h$. If we neglect inter-valley disorder scattering and account for spin degeneracy and valley degeneracy, this DFM result can be compared with graphene experimental results. We see that both the constant mobility and the shift in σ_{\min} suggest long-range scattering similar to that produced by Coulombic impurities. We note that Coulombic impurities in the substrate that are separated from the graphene sheet by a distance that is large compared to the graphene lattice constant but small compared to the Fermi wavelength will act like Coulomb scatterers in the DFM but will not produce strong inter-valley scattering.

The smooth conductivity curves in Fig.1(a) and 1(b) are based on averages over approximately 10^4 disorder realizations. For each disorder realization the conductivity is averaged over a Fermi energy window containing approximately 5-10 levels. To illustrate the statistical character of conductivity near the Dirac point, we plot the disorder averaged Kubo conductivity as a function of η for three different sizes in Fig.1(c). The error bars indicate the scale of fluctuations associated with changing the number of states in the finite systems by ~ 1 . Note that the mean value is close to e^2/h . Fig.1(e) summarizes our results for the Thouless conductivity at the Dirac point. The overall distribution function demonstrates that $\sigma_{T\min}$ is narrowly peaked near e^2/h . The dependence on the density of Coulomb scatterers is indicated by the scatter plot which shows conductivity values calculated at particular n_i values. These results suggest that the DFM σ_{\min} for Coulomb scatterers equals e^2/h to within approximately 15%. For the short-range scatterers case, on the other hand, $\sigma_{T\min} \simeq (1/\pi)e^2/h$.

The difference between Coulomb and short-range disorder σ_{\min} values can be explained qualitatively by the following argument. In the short-range case, the golden-rule mean-free path for delta-function scatterers diverges ($l_0 \propto 1/E_F \rightarrow \infty$) at the Dirac point, which suggests that the $E = 0$ state is always in the clean limit. Indeed, it is significant to note that the universal conductivity at the Dirac point in this model is equal to the conductivity of a disorder-free system[6, 7]. (The conductivity is finite in the absence of scattering because the density of states vanishes at the Dirac point.) In contrast, Boltzmann transport theory suggests that the Dirac point of the Coulomb scatterer model is in the strong disordered limit because $l_c \rightarrow 0$. As long as these states remain delocalized, however, the conductivity cannot vanish; the non-zero conductivity at the Dirac point is purely due to the quantum mechanical nature of delocalized states. Although this argument cannot provide a numerical estimate for the Coulomb case, it indicates that there is an

essential difference between these two cases. A related difference is also seen in the inset in Fig.1(a) which compares densities of states near the Dirac point ($E = 0$) for short-range scatterers (green dashed line) and Coulomb scatterers (blue solid line). The prominent dip at $E = 0$ in the short-range case is replaced by a smooth minimum at a larger value in the Coulomb case. One interpretation of the increase in Dirac point density of states is that the carrier density fluctuates spatially in the smooth Coulomb potential. Non-zero local carrier densities could explain both the increase in density of states and the increase in conductivity.

Quantum interference effects – Finally we address DFM quantum interference effects. The suppressed weak-(anti)localization correction in the doped region is the third striking experimental finding that requires clarification. Prior to the first experiments, a diagrammatic study of quantum corrections to the conductivity of doped graphene concluded[21] that weak localization and weak-antilocalization should occur when the phase coherence length is respectively longer than and shorter than the intervalley scattering length. The Dirac model Coulomb scatterer numerical results illustrated in Fig.1(d), which apply to graphene only when intervalley scattering can be neglected, are consistent with the Dirac model diagrammatic theory result: $\sigma(L) = \sigma_0 + \delta\sigma(L)$ where $\delta\sigma(L) = (2e/\pi\hbar) \log(L/l_c)$ is the weak antilocalization correction and σ_0 is the Boltzmann conductivity[21]. Motivated by experiment, several theoretical studies have been completed more recently which analyze in addition the role of higher order terms in the $\mathbf{k} \cdot \mathbf{p}$ expansion but reached broadly similar conclusions[24].

An alternate possibility, suggested in the original experimental paper, is that quantum corrections are suppressed by ripples in the graphene sheets which can be represented by a random vector potential[23, 28, 29, 30]. To model such distorted graphene we study the Hamiltonian[26]

$$H = -i\hbar v \boldsymbol{\sigma} \cdot [\nabla + i\mathbf{A}(\mathbf{r})] + V(\mathbf{r}). \quad (4)$$

where \mathbf{A} is a random vector potential. For simplicity we choose[28, 29, 30] the following random vector potential model: $\mathbf{A}(\mathbf{r}) = \sum_{J=1}^{N_j} \lambda_J (\hat{\mathbf{z}} \times (\mathbf{r} - \mathbf{R}_J)) / |\mathbf{r} - \mathbf{R}_J|^2 = \sum_{J=1}^{N_j} \lambda_J \nabla \theta(\mathbf{r} - \mathbf{R}_J)$. Here \mathbf{R}_J is the position of J th defect, and λ_J is a coupling constant with random sign, $\theta(\mathbf{r})$ is the angle between \mathbf{r} and x -axis. We find that the random vector potential does indeed suppress the Dirac model's weak-antilocalization as illustrated in Fig.1(c). These results were obtained for a model with equal numbers of Coulombic and topological defects and comparable strengths of the two interactions: ($\langle \lambda_j^2 \rangle = g^2$). In this regime, the minimum conductivity at the Dirac point remains around e^2/h . When the random vector potential dominates over the Coulomb potential, on the other

hand, σ can be smaller than e^2/h at the Dirac point, and closer to $(1/\pi)e^2/h$.

Discussion – We have studied zero-field transport phenomena of two-dimensional massless DFM's by evaluating the finite size Kubo formula, comparing the Coulomb and short-range scatterer cases. The two-component Dirac fermion model is applicable to graphene if intervalley scattering plays a negligible role. We find that Dirac fermion system with Coulomb scatterers are able to account (although probably not uniquely) for two key experimental findings, namely that the conductivity is proportional to carrier density away from the Dirac point and that the minimal conductivity per channel is close to e^2/h , several times larger than the universal value obtained theoretically for short-range scatterers. In the Coulomb case, disorder remains important at the Dirac point. The impurity density n_i in the Coulomb model should be thought of as the density of Coulomb scatterers that are located, not necessarily in, but within a Fermi wavelength of the graphene plane. In this interpretation, the mobilities measured in current samples[14, 15] corresponds to $n_i \simeq 5 \times 10^{11} [\text{cm}^2]$.

We have also studied a simple model intended to represent the effect of ripples in the graphene sheet, which like the Coulombic model gives a conductivity proportional to density. This model is able to account for another key experimental finding, namely that the weak antilocalization of two-dimensional Dirac fermion system is suppressed in graphene. Weak antilocalization in this system can be understood as a Berry phase effect in the momentum space[21, 36], which changes constructive interference of back-scattered particles into destructive interference. We represent topological defects by random vector potentials, leading to a model similar to the ones studied in Refs.7, 17, 34, 35. The random vector potential model can account for the suppressed weak localization[23, 26] seen experimentally. We note that the vector potentials are unscreened even in the doped regime unlike Coulomb scattering, so that Coulomb scattering could dominate at the Dirac point and topological scattering at larger doping. This scenario would provide a consistent explanation for all three experimental findings. We caution however that current experiments cannot rule out an important role for intervalley scattering in graphene, although it appears that conductivity proportional to carrier density in the Boltzmann regime suggests dominant smooth intra-valley scattering that could be Coulombic or topological in character. We note that intervalley scattering is much more likely to be relevant for weak localization corrections, where it need only compete with the phase coherence length, than for Boltzmann transport where it needs to compete with the mean-free-path. These numerical findings, along the future experiments, should enable a definitive explanation for graphene's surprising $B = 0$ transport properties.

Acknowledgment – The authors acknowledge helpful

interactions with A. Geim, T. Hughes, Z. Jiang, P. Kim, E. Komatsu, V. Falko and A. Castro-Neto. This work has been supported by the Welch Foundation and by the Department of Energy under grant DE-FG03-02ER45958.

- [1] J. C. Slonczewski and P. R. Weiss, Phys. Rev. **109**, 272 (1958).
- [2] S. Deser, R. Jakiew, and S. Templeton, Phys. Rev. Lett. **48**, (1982) 975.
- [3] G.W. Semenoff, Phys. Rev. Lett. **53**, 2449 (1984)
- [4] E. Fradkin, E. Dagotto D. Boyanovsky, Phys. Rev. Lett. **57**, (1986) 2967.
- [5] F.D.M. Haldane, Phys. Rev. Lett. **61**, 2015 (1988);
- [6] E. Fradkin, Phys. Rev. B **33**, 3263 (1986)
- [7] A. W. W. Ludwig, M. P. A. Fisher, R. Shankar, and G. Grinstein, Phys. Rev. B 50, 7526 (1994).
- [8] Y. Hatsugai and P. A. Lee, Phys. Rev. B **48**, 4204 (1993).
- [9] C. de C. Chamon *et al.*, Phys. Rev. Lett. **77**, 4194 (1996).
- [10] D.H. Kim *et al.*, Phys. Rev. Lett. **79**, 2109 (1997).
- [11] D. V. Khveshchenko, Phys. Rev. Lett. **87**, 206401 (2001); J. Gonzalez *et al.*, Phys. Rev. B **63**, 134421 (2001); T. Stauber *et al.*, Phys. Rev. B **71**, 041406 (2005); Khveshchenko, cond-mat/0604180.
- [12] P.A. Lee, Phys. Rev. Lett. **71**, 1887 (1993).
- [13] Novoselov *et al.*, Science **306**, 666 (2004).
- [14] K.S. Novoselov *et al.*, Nature **438**, 197 (2005)
- [15] Y.B. Zhang *et al.*, Nature **438**, 201 (2005).
- [16] Adriann M.J. Schakel, Phys. Rev. D **43**, 1428 (1991); Y. Zheng and T. Ando, Phys. Rev. B **65**, 245420 (2002); V.P. Gusynin and S.G. Sharapov, Phys. Rev. Lett. **95**, 146801 (2005); N. M. R. Peres, F. Guinea, A. H. Castro Neto, Phys. Rev. B 73, 125411 (2006).
- [17] Y. Morita and Y. Hatsugai, Phys. Rev. Lett. **79**, 3728-3731 (1997)
- [18] K. Ziegler, Phys. Rev. Lett. **80**, 3113 (1998)
- [19] N.H. Shon and T. Ando, J. Phys. Soc. Jpn. **67** (1998) 2421.
- [20] N. M. R. Peres, F. Guinea, A. H. Castro Neto, Phys. Rev. B **73**, 125411 (2006).
- [21] H. Suzuura and T. Ando, Phys. Rev. Lett. **89**, 266603 (2002).
- [22] P.A. Lee and T.V. Ramakrishnan, Rev. Mod. Phys. **57**, 287 (1985).
- [23] S.V. Morozov, K.S. Novoselov, M.I. Katsnelson, F. Schedin, D. Jiang, A.K. Geim, cond-mat/0603826.
- [24] E. McCann, K. Kechedzhi, Vladimir I. Fal'ko, H. Suzuura, T. Ando, B.L. Altshuler, cond-mat/0604015; D.V.Khveshchenko, cond-mat/0602398.
- [25] K. Nomura, A.H. MacDonald, cond-mat/0604113.
- [26] A. F. Morpurgo, F. Guinea, cond-mat/0603789; J. Gonzalez, F. Guinea, M. A. H. Vozmediano, Phys. Rev. B, **63**, 134421 (2001).
- [27] R. Tamura and M. Tsukada, Phys. Rev. B **52**, 6015 (1995).
- [28] P.E. Lammert, V.H. Crespi, Phys. Rev. Lett. **85**, 5190 (2000).
- [29] D.V. Kolesnikov and V.A. Osipov, Eur. Phys. J. B **49**, 465 (2006).
- [30] A. Cortijo, M. A. H. Vozmediano, cond-mat/0603624.
- [31] D. J. Thouless and S. Kirkpatrick, J. Phys. C, 14, 235

(1981).

- [32] Y. Imry, *Introduction to Mesoscopic Physics*, Oxford University.
- [33] T. Ando, J. Phys. Soc. Jpn. **52**, 1740 (1983); **53** 3101 (1984).
- [34] Y. Hatsugai, X.-G. Wen, and M. Komoto, Phys. Rev. B **56**, 1061 (1997).
- [35] C. Mudry, S. Ryu, and A. Furusaki, Phys. Rev. B **67**, 064202 (2003).
- [36] T. Ando, T. Nakanishi, R. Saito, J. Phys. Soc. Jpn. **67**, 2857 (1998).